Inorg. Chem. **2009**, *48*, 2128−2135

Two-Step Spin-Transition Iron(III) Compound with a Wide [High Spin-Low Spin] Plateau

Jinkui Tang,[†,‡] José Sánchez Costa,[†] Simon Smulders,[†] Gábor Molnár,[§] Azzedine Bousseksou,[§] Simon J. Teat,[||] Yangguang Li,[⊥] Gerard A. van Albada,[†] Patrick Gamez,[*,†] and Jan Reedijk[*,†]

Leiden Institute of Chemistry, Leiden University, P.O. Box 9502, 2300 RA Leiden, The Netherlands, State Key Laboratory of Rare Earth Resource Utilization, Changchun Institute of Applied Chemistry, Chinese Academy of Sciences, Changchun 130022, P.R. China, Laboratoire de Chimie de Coordination, UPR 8241 CNRS, 205 Route de Narbonne, 31077 Toulouse, France, ALS, Berkeley Laboratory, 1 Cyclotron Road, MS2-400, Berkeley, California 94720, and Key Laboratory of Polyoxometalate Science of Ministry of Education, Institute of Polyoxometalate Chemistry, Department of Chemistry, Northeast Normal University, Changchun, 130024, P.R. China

Received October 16, 2008

A new iron(III) coordination compound exhibiting a two-step spin-transition behavior with a remarkably wide [HS-LS] plateau of about 45 K has been synthesized from a hydrazino Schiff-base ligand with an N,N,O donor set, namely 2-methoxy-6-(pyridine-2-ylhydrazonomethyl)phenol (**Hmph**). The single-crystal X-ray structure of the coordination compound $\{[Fe(\mathbf{mph})_2](ClO_4)(MeOH)_{0.5}(H_2O)_{0.5}\}_2$ (**1**) determined at 150 K reveals the presence of two slightly different iron(III) centers in pseudo-octahedral environments generated by two deprotonated tridentate **mph** ligands. The presence of hydrogen bonding interactions, instigated by the well-designed ligand, may justify the occurrence of the abrupt transitions. **1** has been characterized by temperature-dependent magnetic susceptibility measurements, EPR spectroscopy, differential scanning calorimetry, and ^{57}Fe Mössbauer spectroscopy, which all confirm the occurrence of a two-step transition. In addition, the iron(III) species in the high-spin state has been trapped and characterized by rapid cooling EPR studies.

Introduction

The near-equivalence of the ligand-field splitting parameter and the spin-pairing energy for a variety of d^4-d^7 transition metal coordination compounds produces quasi-degenerate high-spin (HS) and a low-spin (LS) electronic states.[1] In these compounds, the so-called spin-crossover (SCO) phenomenon can be induced by the variation of temperature, pressure, magnetic field, or light.[2−5] The first case of SCO was observed by Cambi et al. in 1931 for an iron(III) compound.[6,7] Since this pioneering work, many iron-based SCO systems have been developed.[8−10] Most of the examples reported involved iron(II) compounds.[1,11] However, iron(III) SCO compounds are fairly documented as well.[12−19] The growing interest in the development of SCO compounds is connected with the increasing awareness that this phenomenon may find potential applications in molecular electronics

* To whom correspondence should be addressed. E-mail: reedijk@chem.leidenuniv.nl. Fax: +31 715274671.
† Leiden University.
‡ Chinese Academy of Sciences.
§ Laboratoire de Chimie de Coordination, UPR 8241 CNRS.
|| ALS, Berkeley Laboratory.
⊥ Northeast Normal University.

(1) *Spin Crossover in Transition Metal Compounds I-III*; Gütlich, P.; Goodwin, H. A., Eds.; Springer-Verlag Berlin: Berlin, 2004; Vols. *233−235*.
(2) Garcia, Y.; Ksenofontov, V.; Levchenko, G.; Schmitt, G.; Gütlich, P. *J. Phys. Chem. B* **2000**, *104*, 5045–5048.
(3) Bousseksou, A.; Boukheddaden, K.; Goiran, M.; Consejo, C.; Boillot, M. L.; Tuchagues, J. P. *Phys. Rev. B* **2002**, *65*, 172412.
(4) Decurtins, S.; Gütlich, P.; Köhler, C. P.; Spiering, H.; Hauser, A. *Chem. Phys. Lett.* **1984**, *105*, 1–4.
(5) Bousseksou, A.; Molnár, G.; Matouzenko, G. *Eur. J. Inorg. Chem.* **2004**, 4353–4369.
(6) Cambi, L.; Szegö, L. *Ber.* **1931**, *64*, 2591–2598.
(7) Cambi, L.; Cagnasso, A. *Atti. Accad. Naz. Lincei, Cl. Sci. Fis. Mat. Nat. Rend.* **1931**, 809.
(8) Halcrow, M. A. *Chem. Soc. Rev.* **2008**, *37*, 278–289.
(9) Gütlich, P.; Garcia, Y.; Goodwin, H. A. *Chem. Soc. Rev.* **2000**, *29*, 419–427.
(10) Kahn, O.; Codjovi, E. *Philos. Trans. R. Soc., A* **1996**, *354*, 359–379.
(11) Bousseksou, A.; Molnár, G.; Real, J. A.; Tanaka, K. *Coord. Chem. Rev.* **2007**, *251*, 1822–1833.

10.1021/ic801973x CCC: $40.75
Published on Web 02/03/2009

Chart 1

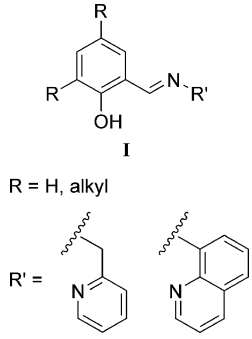

(fabrication of switching, sensing and memory devices), thus making this field relevant to various areas of research investigations in chemistry, solid-state physics, and even biology.

In contrast to Iron(II) SCO compounds, Iron(III) SCO compounds have the great advantage to be usually air-stable, facilitating their handling and study. Indeed, iron(II) SCO compounds may lose their spin-transition properties upon oxidation of Fe^{II} centers to Fe^{III}, which is obviously not taking place with iron(III) coordination compounds. A number of Schiff-base ligands (typically containing at least one N,N,O donor set) have been successfully used to generate pseudo-octahedral Fe^{III} compounds exhibiting SCO properties.[20−25] In particular, tridentate Schiff-base ligands of type I (Chart 1) have been comprehensively investigated.[26−29]

Recently, an interesting two-step SCO system obtained from iron(III) perchlorate and the ligand **Hsalpm** (Chart 2) has been described.[30] On the basis of these earlier results,

Chart 2

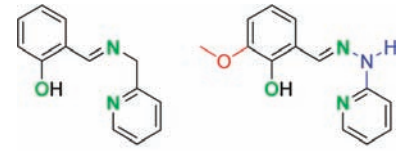

the perchlorate iron(III) coordination compound from the related ligand 2-methoxy-6-(pyridine-2-ylhydrazonomethyl)phenol (**Hmph**, Chart 2), which contains both one hydrogen-donor group (in blue in Chart 2) and one hydrogen-acceptor group (in red in Chart 2) near the donor atoms (in green in Chart 2), has been synthesized (compare **Hsalpm** and **Hmph** in Chart 2) to investigate the influence of hydrogen-bonding interactions on the SCO properties. It is indeed well-known that the coexistence of short- and long-range interactions, of mainly elastic origin, between molecules induces cooperative phenomena such as first-order phase transitions[31] or two-step transitions.[32,33] Actually, the ligand **Hmph** has been used earlier to prepare iron(III) SCO coordination compounds with PF_6^- and BPh_4^- as counterions.[34] However, the structural features of these two compounds could not be described as their X-ray molecular structures were not determined.

In this Article, the preparation and full characterization of an iron(III) coordination compound obtained from **Hmph** and $Fe(ClO_4)_2$ are described. The structural features and the magnetic properties of the new compound $\{[Fe(\mathbf{mph})_2](ClO_4)(MeOH)_{0.5}(H_2O)_{0.5}\}_2$ (**1**) are compared to those of the analogous compound $[Fe(\mathbf{salpm})_2]ClO_4 \cdot 0.5EtOH$ reported by Shongwe et al.[30]

Experimental Section

Materials. All chemicals purchased were reagent grade and used without further purification. The ligand 2-methoxy-6-(pyridine-2-ylhydrazonomethyl)phenol (**Hmph**) was synthesized according to a procedure described earlier.[34,35]

$\{[Fe(mph)_2](ClO_4)(MeOH)_{0.5}(H_2O)_{0.5}\}_2$ (1). A solution of 61 mg (0.25 mmol) of Hmph in 5 mL of methanol was added to a solution of 181 mg (0.5 mmol) of $Fe(ClO_4)_2 \cdot 6H_2O$ in 5 mL of methanol. A black precipitate formed immediately which was removed by filtration. The resulting green filtrate was left unperturbed to allow slow evaporation of the solvent under air. Dark-orange crystals, suitable for X-ray diffraction analysis, were formed after 1 week. The formation of iron(III) resulted from the aerial oxidation of the initial iron(II). Yield: 38 mg, 46% (based on the ligand Hmph). Anal. Calcd for $C_{26.5}H_{27}ClFeN_6O_9$ (Mw = 664.83 g mol^{-1}): C, 47.87; H, 4.09; N, 12.64. Found: C, 47.84; H, 3.88; N, 12.23%. FT-IR (cm^{-1}, neat): 1620, 1538, 1428, 1348, 1285, 1250, 1218, 1142, 1070, 968, 856, 768, 744, 734, 621, 510, 430, 398.

(12) Ando, H.; Nakao, Y.; Sato, H.; Sakaki, S. *J. Phys. Chem. A* **2007**, *111*, 5515–5522.
(13) Floquet, S.; Guillou, N.; Negrier, P.; Riviere, E.; Boillot, M. L. *New J. Chem.* **2006**, *30*, 1621–1627.
(14) Singhal, S.; Garg, A. N.; Chandra, K. *Transition Met. Chem.* **2005**, *30*, 44–52.
(15) Kersting, B.; Kolm, M. J.; Janiak, C. *Z. Anorg. Allg. Chem.* **1998**, *624*, 775–780.
(16) Zelentsov, V. V. *Russ. J. Coord. Chem.* **2003**, *29*, 425–430.
(17) Fettouhi, M.; Morsy, M.; Waheed, A.; Golhen, S.; Ouahab, L.; Sutter, J. P.; Kahn, O.; Menendez, N.; Varret, F. *Inorg. Chem.* **1999**, *38*, 4910–4912.
(18) Faulmann, C.; Dorbes, S.; de Bonneval, W. G.; Molnar, G.; Boussekssou, A.; Gomez-Garcia, C. J.; Coronado, E.; Valade, L. *Eur. J. Inorg. Chem.* **2005**, 3261–3270.
(19) van Koningsbruggen, P. J.; Maeda, Y.; Oshio, H. *Top. Curr. Chem.* **2004**, *233*, 259–324.
(20) Hayami, S.; Miyazaki, S.; Yamamoto, M.; Hiki, K.; Motokawa, N.; Shuto, A.; Inoue, K.; Shinmyozu, T.; Maeda, Y. *Bull. Chem. Soc. Jpn.* **2006**, *79*, 442–450.
(21) Klein, M.; Renz, F. *Hyperfine Interact.* **2006**, *168*, 1001–1007.
(22) Boca, R.; Fukuda, Y.; Gembicky, M.; Herchel, R.; Jarosciak, R.; Linert, W.; Renz, F.; Yuzurihara, J. *Chem. Phys. Lett.* **2000**, *325*, 411–419.
(23) Timken, M. D.; Hendrickson, D. N.; Sinn, E. *Inorg. Chem.* **1985**, *24*, 3947–3955.
(24) Hernández-Molina, R.; Mederos, A.; Dominguez, S.; Gili, P.; Ruiz-Pérez, C.; Castiñeiras, A.; Solans, X.; Lloret, F.; Real, J. A. *Inorg. Chem.* **1998**, *37*, 5102–5108.
(25) Ivanova, T. A.; Ovchinnikov, I. V.; Turanov, A. N. *Phys. Solid State* **2007**, *49*, 2132–2137.
(26) Juhász, G.; Hayami, S.; Sato, O.; Maeda, Y. *Chem. Phys. Lett.* **2002**, *364*, 164–170.
(27) Hayami, S.; Kawahara, T.; Juhasz, G.; Kawamura, K.; Uehashi, K.; Sato, O.; Maeda, Y. *J. Radioanal. Nucl. Chem.* **2003**, *255*, 443–447.
(28) Okamura, S.; Maeda, Y. *J. Radioanal. Nucl. Chem.* **2003**, *255*, 523–528.
(29) Hayami, S.; Gu, Z. Z.; Yoshiki, H.; Fujishima, A.; Sato, O. *J. Am. Chem. Soc.* **2001**, *123*, 11644–11650.
(30) Shongwe, M. S.; Al-Rashdi, B. A.; Adams, H.; Morris, M. J.; Mikuriya, M.; Hearne, G. R. *Inorg. Chem.* **2007**, *46*, 9558–9568.
(31) Spiering, H. *Top. Curr. Chem.* **2004**, *235*, 171–195.
(32) Bousseksou, A.; Nasser, J.; Linares, J.; Boukheddaden, K.; Varret, F. *J. Phys. I* **1992**, *2*, 1381–1403.
(33) Köhler, C. P.; Jakobi, R.; Meissner, E.; Wiehl, L.; Spiering, H.; Gütlich, P. *J. Phys. Chem. Solids* **1990**, *51*, 239–247.
(34) Mohan, M.; Gupta, N. S.; Chandra, L.; Jha, N. K.; Prasad, R. S. *Inorg. Chim. Acta* **1988**, *141*, 185–192.
(35) Tang, J.; Costa, J. S.; Aromí, G.; Mutikainen, I.; Turpeinen, U.; Gamez, P.; Reedijk, J. *Eur. J. Inorg. Chem.* **2007**, 4119–4122.

Physical Measurements. Elemental analyses (C, H, and N) were performed on a Perkin-Elmer 2400 series II analyzer. FT-IR spectra were recorded as neat samples in the range 400−4000 cm^{-1} on a Perkin-Elmer Paragon 1000 FTIR spectrophotometer, equipped with a Golden Gate ATR device. Variable-temperature magnetic susceptibilities were measured on a Quantum Design MPMS-XL-5 SQUID magnetometer (using a magnetic field of 0.5 T and applying a heating and cooling rate of ±1 K min^{-1}; the magnetization was measured every 3 K). Diamagnetic corrections were made with Pascal's constants for all the constituent atoms.[36] X-band electron paramagnetic resonance (EPR) measurements were performed on a Bruker EMX spectrometer. Differential Scanning Calorimetry (DSC) measurements were carried out on a Netzsch DSC 204 instrument under helium purging gas (20 cm^3 min^{-1}) at a scan rate of 10 K min^{-1} in both heating and cooling modes. Temperature and enthalpy were calibrated using the melting transition of standard materials (Hg, In, Sn). The uncertainty in the transition enthalpy (ΔH) and entropy (ΔS) is estimated of about 10 % because of the subtraction of the unknown baseline. ^{57}Fe Mössbauer spectra have been recorded using a conventional constant-acceleration type spectrometer equipped with a 50 mCi ^{57}Co source and a flow-type, liquid nitrogen cryostat. Least square fittings of the Mössbauer spectra have been carried out with the assumption of Lorentzian line shapes using the Recoil software package (http://www.isapp-s.ca/recoil/).

Structural Determination. X-ray crystallographic data for compound **1** were collected at 150(2) K using a Bruker APEX II CCD diffractometer on station 11.3.1 of the Advanced Light Source at Lawrence Berkeley National Laboratory, at 0.7749 Å, from a Silicon 111 monochromator. The data were cut at 0.86 Å as $I/\sigma <$ 2 and therefore on average unobserved. The structure was solved by direct methods using SIR97[37] through WinGX[38] and refined by the SHELXTL[39] suite of programs. All atoms were refined anisotropically except the disordered perchlorate oxygen atoms and the water molecules with partial occupancy. The hydrogen atoms for the methyl and hydroxyl groups were found in the difference map and constraints while for the other carbon atoms they were placed geometrically. All these H atoms were refined using a riding model. The hydrogen atoms on the nitrogen atoms were found in the difference map and allowed to refine freely. The hydrogen atoms could be neither placed nor found on the water molecules and were therefore omitted from the refinement. Geometrical and displacement parameter restrains were used to model the perchlorate anions.

HS Trapping in the Magnetic Susceptibility Measurements. A rapid cooling, trapping experiment was carried in the SQUID magnetometer. A polycrystalline sample of **1** was rapidly quenched at 6 K in the SQUID cavity. After stabilization of the temperature, the observed $\chi_M T$ value was 0.65 cm^3 K mol^{-1}. Hence, following a reported procedure,[40] the sample was heated at a constant rate of 1 K min^{-1}, showing that the trapped HS species were stable up to 33 K (see Figure 5). To estimate the percentage of Fe(III) HS species trapped, it has been considered that, at room temperature, HS **1** exhibits a $\chi_M T$ value of 4.26 cm^3 K mol^{-1}. In addition, LS **1** shows a $\chi_M T$ value of 0.48 cm^3 K mol^{-1} at 6 K. From these HS and LS $\chi_M T$ values and the one obtained by rapid cooling of the sample at 6 K, the percentage of trapped Fe(III) species could be calculated, which corresponds to about 7% of the initial HS **1**.

(36) Kahn, O. *Molecular Magnetism*; VCH: New York, 1993.
(37) Altomare, A.; Burla, M. C.; Camalli, M.; Cascarano, G. L.; Giacovazzo, C.; Guagliardi, A.; Moliterni, A. G. G.; Polidori, G.; Spagna, R. *J. Appl. Crystallogr.* **1999**, *32*, 115–119.
(38) Farrugia, L. J. *J. Appl. Crystallogr.* **1999**, *32*, 837–838.
(39) *SHELXTL*; Bruker AXS: Madison, WI, 2007.
(40) Létard, J. F.; Chastanet, G.; Nguyen, O.; Marcen, S.; Marchivie, M.; Guionneau, P.; Chasseau, D.; Gütlich, P. *Monatsh. Chem.* **2003**, *134*, 165–182.

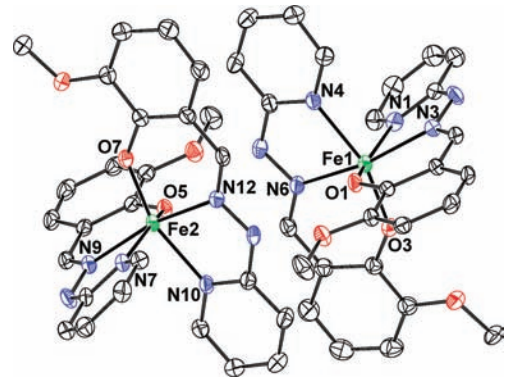

Figure 1. ORTEP representation at the 30% probability level of the cationic part of compound $\{[Fe(\mathbf{mph})_2](ClO_4)(MeOH)_{0.5}(H_2O)_{0.5}\}_2$ (**1**) whose crystal structure was determined at 150 K. Hydrogen atoms are omitted for clarity.

Table 1. Selected Bond Distances (Å) and Angles (deg) for $[Fe(\mathbf{mph})_2]_2(ClO_4)_2(CH_3OH)(H_2O)$ (**1**)

Fe1		Fe2	
Fe1−O1	1.937(3)	Fe2−O5	1.925(3)
Fe1−O3	1.887(3)	Fe2−O7	1.883(3)
Fe1−N1	2.147(5)	Fe2−N7	2.167(5)
Fe1−N3	2.136(4)	Fe2−N9	2.120(5)
Fe1−N4	2.153(4)	Fe2−N10	2.152(4)
Fe1−N6	2.144(4)	Fe2−N12	2.131(4)
O1−Fe1−O3	96.89(13)	O5−Fe2−O7	95.40(13)
O1−Fe1−N1	157.36(15)	O5−Fe2−N7	157.58(15)
O1−Fe1−N3	84.23(15)	O5−Fe2−N9	84.34(15)
O1−Fe1−N4	91.36(15)	O5−Fe2−N10	89.55(15)
O1−Fe1−N6	107.49(15)	O5−Fe2−N12	109.83(15)
O3−Fe1−N1	95.33(15)	O7−Fe2−N7	97.20(15)
O3−Fe1−N3	102.36(14)	O7−Fe2−N9	104.23(14)
O3−Fe1−N4	158.17(15)	O7−Fe2−N10	159.11(15)
O3−Fe1−N6	84.09(14)	O7−Fe2−N12	84.72(14)
N1−Fe1−N3	74.55(17)	N7−Fe2−N9	74.63(17)
N1−Fe1−N4	84.18(16)	N7−Fe1−N10	85.26(16)
N1−Fe1−N6	92.67(17)	N7−Fe2−N12	89.78(17)
N3−Fe1−N4	98.55(16)	N9−Fe2−N10	96.44(16)
N3−Fe1−N6	166.05(17)	N9−Fe2−N12	162.74(17)
N4−Fe1−N6	74.15(16)	N10−Fe2−N12	74.53(16)

Results and Discussion

Structural Description. The reaction of iron(II) perchlorate with 2-methoxy-6-(pyridine-2-ylhydrazonomethyl)phenol (**Hmph**)[35] in methanol produces the mononuclear compound $\{[Fe(\mathbf{mph})_2](ClO_4)(MeOH)_{0.5}(H_2O)_{0.5}\}_2$ (**1**), whose molecular structure determined at 150(2) K is depicted in Figure 1. It has to be noticed that the initial iron(II) has been oxidized to iron(III) under aerobic conditions.

1 crystallizes in the triclinic $P\bar{1}$ space group. Selected bond lengths and angles are given in Table 1 and crystal parameters are shown in Table 2. The crystal lattice of this compound is composed of two slightly different iron(III) centers identified as Fe1 and Fe2 (Figure 1). The coordination environment of both metal centers is distorted octahedral, constituted by two deprotonated **mph** ligands, resulting in $Fe^{III}N_4O_2$ chromophores. The distortion of the O_h geometry is most likely imposed by the two chelate angles of the tridentate, N,N,O **mph** ligand (the N−Fe−N angles vary from 74.15(16) to 74.63(17)°, and the N−Fe−O from

Table 2. Crystal Data and Structure Refinement for Compound **1**

$[Fe(\mathbf{mph})_2]_2(ClO_4)_2(CH_3OH)(H_2O)$	
empirical formula	$C_{26.5}H_{27}ClFeN_6O_9$
F_w (g mol^{-1})	664.84
crystal system	triclinic
space group	$P\bar{1}$
crystal color	dark orange
temperature (K)	150(2)
a (Å)	12.932(2)
b (Å)	15.096(2)
c (Å)	15.345(2)
α (deg)	95.397(2)
β (deg)	99.435(2)
γ (deg)	91.806(2)
V (Å^3)	2938.7(7)
ρ_{calcd} (Mg/m^3)	1.503
μ (mm^{-1})	0.667
$F(000)$	1372
θ for data collection (deg)	2.75−26.26
collected reflections	26 158
Independent reflections	9670
R_{int}	0.0499
R [$I > 2\sigma(I)$]	0.0555
wR (all data)	0.1729
goodness of fit on F^2	1.007
largest diff. peak and hole (e Å^3)	0.645 and −0.663

84.09(14) to 84.72(14)°; Table 1). The Fe−O and Fe−N bond lengths are comparable for both iron centers (see Table 1). The average coordination bond distances in **1** are Fe−$O_{phenolate}$: 1.908(3) Å, Fe−N_{imine}: 2.133(4) Å and Fe−N_{pyr}: 2.155(5) Å. As reported by Shongwe et al.,[30] typical Fe−$O_{phenolate}$, Fe−N_{imine}, and Fe−$N_{pyridyl}$ bond lengths in related hexacoordinate $Fe^{III}N_4O_2$ SCO compounds are in the ranges 1.895−1.938, 2.051−2.155, 2.168−2.24 Å for the HS state and 1.850−1.885, 1.905−1.961, and 1.993−2.024 Å for the LS state.[30] Actually, at 150 K the present system is characterized by a ratio HS/LS of about 35/65 (see Magnetic Susceptibility Measurements below). Moreover, as revealed by Mössbauer spectroscopy, there is only one type of HS and LS species (see Mössbauer spectroscopy below). These features therefore suggest that Fe1 and Fe2 behave as identical SCO centers which simultaneously undergo the spin transition upon cooling, resulting in an intermediate state [$Fe1^{HS}$/$Fe1^{LS}$-$Fe2^{HS}$/$Fe2^{LS}$], which is reflected by the similar Fe1−L and Fe2−L coordination bond distances observed for **1** at 150 K (Table 1). On the basis of the normal bond distances found for similar $Fe^{III}N_4O_2$ compounds in the HS and LS states (see above),[30] Fe−$O_{phenolate}$, Fe−N_{imine}, and Fe−$N_{pyridyl}$ bond lengths in the ranges 1.866−1.904, 1.956−2.029, and 2.054−2.094 Å are expected for a HS/LS mixture of 35/65. It thus appears that the corresponding Fe−$O_{phenolate}$, Fe−N_{imine}, and Fe−N_{pyr} distances of respectively 1.908(3), 2.133(4), and 2.155(5) Å in **1** are somewhat above the estimated ranges (by 0.004, 0.104, and 0.061 Å, respectively). Attempts have been made to obtain the molecular structure of **1** at different temperatures, namely 110, 140, 180, 215, and 296 K, to investigate the variations of the coordination bond lengths upon spin crossover. Unfortunately, not sufficient X-ray diffraction data could be obtained. However, these data have allowed the determination of the unit cell parameters for **1** at these five temperatures, which reveal interesting features. First, the space group, that is, triclinic P, is maintained at all temperatures. Plots of

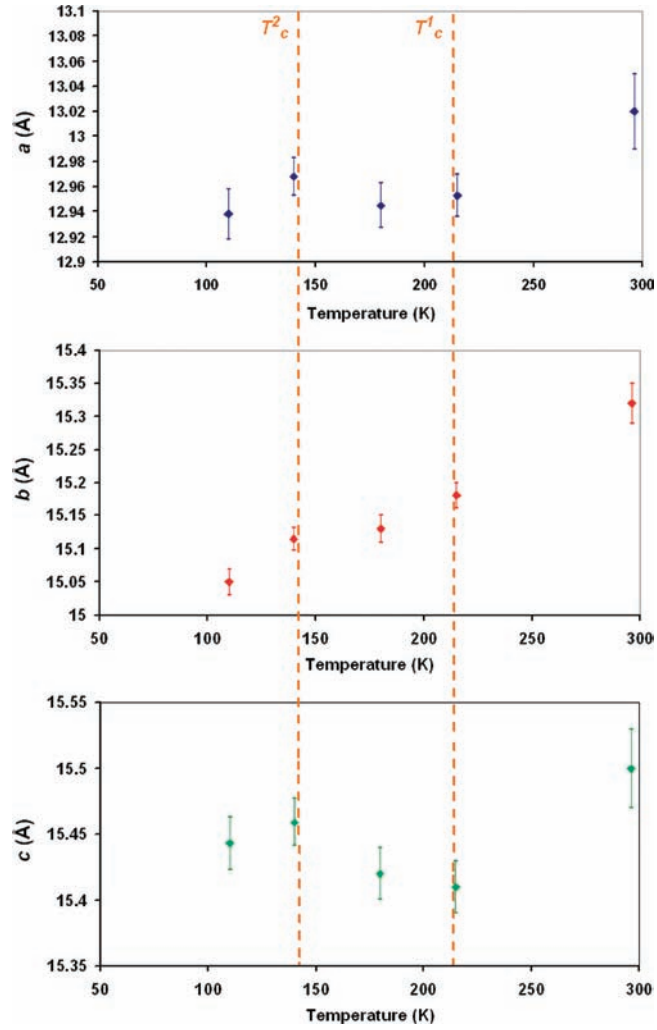

Figure 2. Plots of the cell dimensions a (Å), b (Å), and c (Å) for **1** determined at 110, 140, 180, 215, and 296 K. The dotted lines characterize the transition temperatures determined by magnetic susceptibility measurements.

cell dimension versus temperature are depicted in Figures 2, 3 and Supporting Information, Figure S1. The unit cell parameters a, b, and c (Figure 2) clearly decrease upon the first step of the transition. Surprisingly, the variation of a and c shows a significant increase of these parameters when the second step of the transition takes place, while the expected decrease is observed for b. Therefore, an expansion of the unit cell along the a and c axes (see Supporting Information, Figure S2 for the unit cell axes) occurs when **1** undergoes the second step of the transition. In fact, the a and c axes are in the direction of the two perpendicular **mph** ligands coordinated to the metal centers, and the b axis is along the two interacting iron(III) units (Fe1 and Fe2; Supporting Information, Figure S2). Therefore, the diminution of b with the temperature suggests that the two iron(III) molecules are getting closer to each other when the two-step transition arises. This enhanced closeness of the Fe1 and Fe2 units probably results in an increase of steric constraints, which are most likely counterbalanced by the elongation of the coordination bonds (reflected by the increase of the a and c parameters), when the second step occurs. A similar behavior is noticed for the cell angles α,

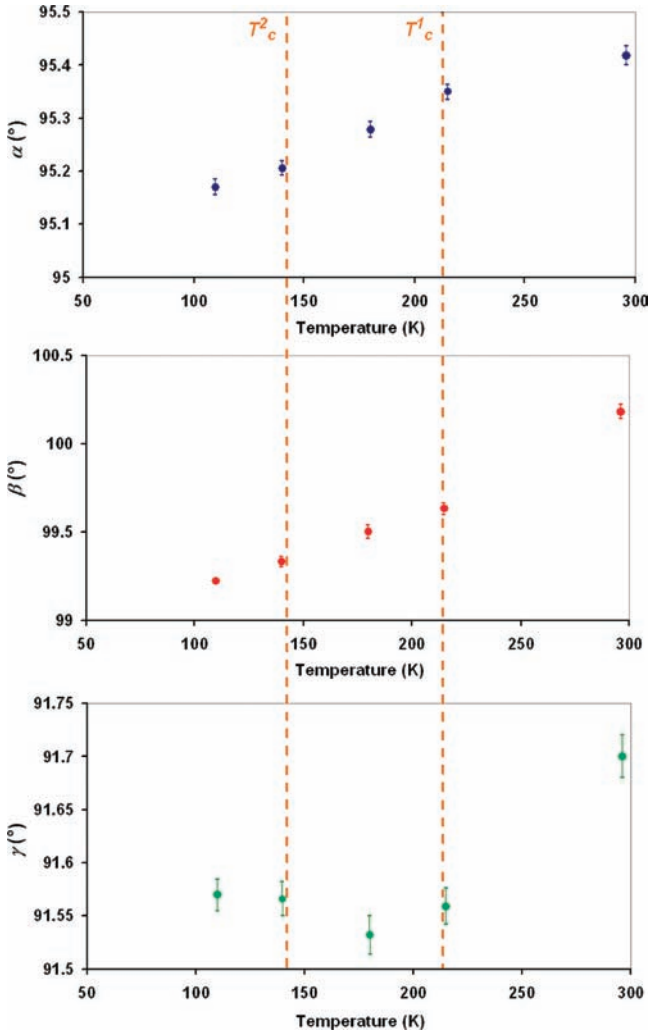

Figure 3. Plots of the cell dimensions α (deg), β (deg), and γ (deg) for **1** determined at 110, 140, 180, 215, and 296 K. The dotted lines characterize the transition temperatures determined by magnetic susceptibility measurements.

β, and γ (Figure 3). However, in that case, two parameters, that is, α and β, follow the transition while γ shows an increase at the second transition. The variation of the unit cell volume with the temperature (Supporting Information, Figure S2) is indicative as well of a structural modification during the second transition step.

This significant difference of SCO behavior compared with that of the closely related compound [Fe(**salpm**)$_2$]ClO_4·0.5EtOH[30] can be explained by the hydrogen bonding network observed in the crystal structure of **1** (Figure 4). As mentioned above (see Introduction), the ligand **Hmph** presents both a hydrogen-donor and a hydrogen-acceptor moieties. Therefore, the solid-state structures of [Fe(**salpm**)$_2$]-ClO_4·0.5EtOH[30] and **1** at 150 K have been closely examined (Figure 4). The sole difference between the two structurally related $[FeN_4O_2]^+$ units is the presence of a hydrogen bond donor (N−H group) and a hydrogen bond acceptor (O-Me group) in the ligand **Hmph** (these groups are absent in **Hsalpm**, Chart 2). As expected, these functional groups are involved in hydrogen-bonding interactions (Table 3). In the crystal lattice, the iron(III) complex cations form molecular pairs by means of four hydrogen bonds (Figure 4B; Table 3). Similarly to [Fe(**salpm**)$_2$]ClO_4·0.5EtOH,[30] the two iron(III) units in **1** further interact by means of π-π interactions. In addition, these supramolecular dimers are connected to solvent molecules (water for Fe1 and methanol for Fe2, Figure 4B) which in turn are hydrogen bonded to perchlorate anions. This remarkable supramolecular association gives rise to a one-dimensional chain in which the elastic interactions between SCO centers may be favored. In fact, the comparison of the magnetic properties of [Fe(**salpm**)$_2$]ClO_4·0.5EtOH[30] with those of **1** (see Magnetic Susceptibility Measurements below) reveals important disparities. Both [Fe(**salpm**)$_2$]ClO_4·0.5EtOH and **1** exhibit two-step SCO properties. However, the transitions are significantly steeper in **1** than those observed for [Fe(**salpm**)$_2$]ClO_4·0.5EtOH. Moreover, the two spin transitions occur at higher temperatures for **1**, namely 214 and 142 K and are separated by a flat plateau, while the first and second steps are centered at, respectively, 180 and 100 K for [Fe(**salpm**)$_2$]ClO_4·0.5EtOH.[30] It thus appears that the hydrogen bonds indeed promote a better cooperativity between the SCO sites. Actually, this improved cooperativity between the iron centers is clearly evidenced by the fact that both Fe1 and Fe2 undergo a concurrent spin transition. In contrast, in the case of [Fe(**salpm**)$_2$]ClO_4·0.5EtOH,[30] the two crystallographically distinct iron(III) atoms (Fe2 and Fe2_a; Figure 4A) act as independent SCO centers; thus, the HS→LS transition of the Fe2 site does not affect the magnetic properties of the Fe2_a site (there is no interaction between Fe2 and Fe2_a). In **1**, Fe1 and Fe2 are strongly interacting through various hydrogen bonds (Figure 4B). As a result the HS→LS transition of Fe1 strongly influences that of Fe2 and vice versa.

It has to be mentioned as well that the counter-ions may play a crucial role in the SCO behavior of a complex cation. Indeed, Mohan et al. have shown that the spin transitions are different for [Fe(**mph**)$_2$]X with X = PF_6 or BPh_4.[34] The spin transition is gradual and virtually complete for Ph_4B^- whereas it is incomplete for PF_6^-. In the present study, the use of ClO_4^- as counterion gives rise to a two-step transition which is moreover abrupt and complete.

Magnetic Susceptibility Measurements. Figure 5 shows the plot $\chi_M T$ versus T of a polycrystalline sample of **1**. The room-temperature $\chi_M T$ value of 4.25 cm^3 mol^{-1} K characterizes a $^6A_{1g}$ (S = 5/2) ground-state for an iron(III) species in an octahedral coordination environment.[20,41] Upon cooling, the $\chi_M T$ value remains constant until 225 K, where a first abrupt transition is observed (T^1_c = 214 K). The resulting intermediate state (the $\chi_M T$ value is about 2.4 cm^3 mol^{-1} K) is detected from 204 to 159 K. After this large plateau of 45 K, the second abrupt transition occurs, and the $\chi_M T$ value drops to 0.69 cm^3 mol^{-1} K at 126 K (T^2_c = 142 K). Between 126 and 6 K, the $\chi_M T$ value remains constant, around 0.56 cm^3 mol^{-1} K, characterizing an almost complete transition (the spin-only theoretical value expected for a LS ($^2T_{2g}$, S = 1/2) Fe^{III} species with g = 2 is 0.375 cm^3 mol^{-1} K. However, because of the significant orbital contribution to the para-

(41) Ikuta, Y.; Ooidemizu, M.; Yamahata, Y.; Yamada, M.; Osa, S.; Matsumoto, N.; Iijima, S.; Sunatsuki, Y.; Kojima, M.; Dahan, F.; Tuchagues, J. P. *Inorg. Chem.* **2003**, *42*, 7001–7017.

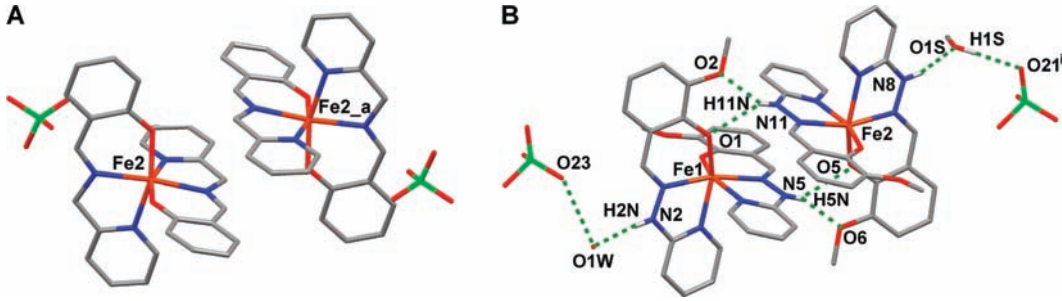

Figure 4. (A) View of two iron(III) centers in the crystal packing of $[Fe(salpm)_2]ClO_4 \cdot 0.5EtOH$ at 150 K;[30] the distance Fe2···Fe2_a = 6.339(4) Å (symmetry operation a: $-x, -y, -z$); (B) View of the two crystallographically independent iron(III) centers in the crystal structure of **1** at 150 K, revealing the hydrogen bonding interactions involving the hydrazino group; the distance Fe1···Fe2 = 5.789(1). For the hydrogen bond distances and angles, see Table 3 (symmetry operation i: $x + 1, y - 1, z$).

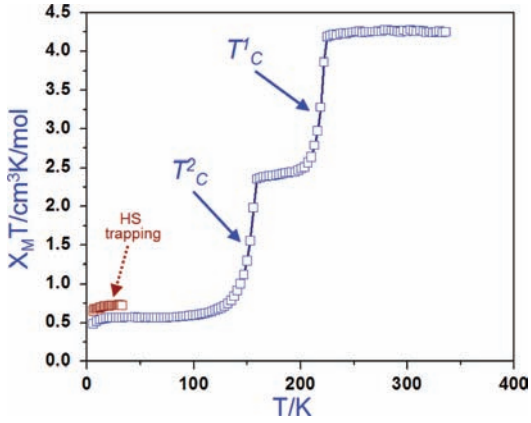

Figure 5. $\chi_M T$ vs T plot for a polycrystalline sample of $\{[Fe(\mathbf{mph})_2](ClO_4)(MeOH)_{0.5}(H_2O)_{0.5}\}_2$ (**1**) after a cooling and a warming cycle.

Table 3. Hydrogen-Bond Geometry in **1**[a]

D−H···A	H···A (Å)	D···A (Å)	D−H−A (deg)
N2−H2N···O1W	0.84(5)	2.821(6)	170(5)
N5−H5N···O5	0.83(6)	2.975(5)	132(5)
N5−H5N···O6	0.83(6)	2.870(6)	154(5)
N8−H8N···O1S	0.80(5)	2.721(6)	164(5)
N11−H11N···O1	0.71(5)	2.999(5)	143(5)
N11−H11N···O2	0.71(5)	2.786(5)	147(5)
O1W···O23		3.011(12)	
O1S−H1S···O21[b]	0.84	2.815(7)	177

[a] See Figure 2. [b] Symmetry codes: (i) $x + 1, y - 1, z$.

magnetism, the $\chi_M T$ value is usually around 0.50 cm^3 mol^{-1} K).[36] The subsequent very slight drop of $\chi_M T$ below 15 K can be attributed to the zero-field splitting of remaining HS Fe^{III} species. Upon heating, the two abrupt transitions occur at the same temperatures; in other words, the spin transition does not show any hysteresis. It is interesting to notice the appearance of two angular points in the transition curve, which is not really consistent with the lack of observable hysteresis. This might be an indication of a structural transition (as suggested as well by the temperature-dependent variation of the unit cell dimensions; see above), which triggers the spin crossover in the iron ions.

EPR Spectroscopic Studies. Since both the LS ($S = 1/2$) and HS ($S = 5/2$) states of iron(III) species are paramagnetic, EPR spectroscopy is one of the potential methods for their characterization.

The EPR measurements were performed in the X band on a polycrystalline sample of **1**. At 70 K, the axial signal observed with $g_\perp = 2.14$ and $g_\parallel = 1.94$ is typical for LS iron(III) centers of this type (Figure 6).[23,30] When the temperature is raised up to 149 K, an additional broad signal is detected around $g = 4.69$ which is attributed to a typical, rhombic HS iron(III) signal (Figure 6).[42,43] The broadening of the signals are most likely due to spin−spin interactions.[44] Next, the spectrum was recorded at 170 K which is a temperature located at the center of the plateau (Figure 5). The two signals at $g = 4.64$ (HS Fe^{III}) and $g = 2.06$ (LS Fe^{III}) appear to be of about equivalent intensity, consistent with a [HS-LS] intermediate state, as evidenced by magnetic susceptibility measurements. At room temperature, the spectrum shows a broad signal centered at $g = 4.64$ and a weak feature around $g = 2.18$. The former signal is ascribed

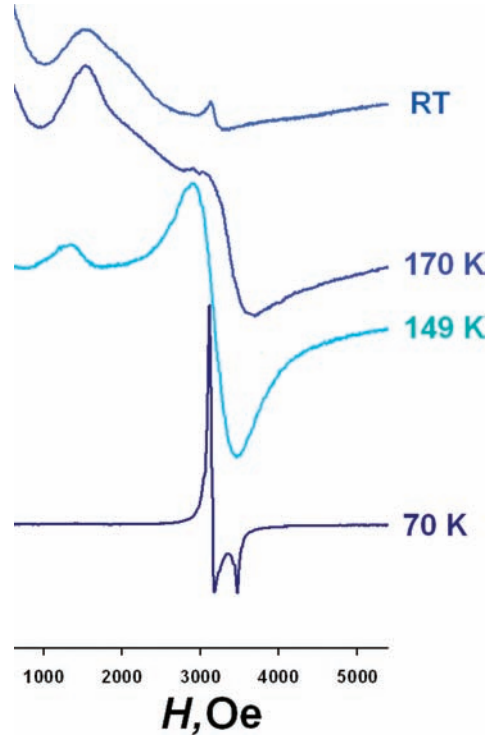

Figure 6. Temperature-dependent X-band EPR spectra of a polycrystalline sample of $\{[Fe(\mathbf{mph})_2](ClO_4)(MeOH)_{0.5}(H_2O)_{0.5}\}_2$ (**1**).

(42) Costes, J. P.; Dahan, F.; Laurent, J. P. *Inorg. Chem.* **1990**, *29*, 2448–2452.
(43) Imbert, C.; Hratchian, H. P.; Lanznaster, M.; Heeg, M. J.; Hryhorczuk, L. M.; McGarvey, B. R.; Schlegel, H. B.; Verani, C. N. *Inorg. Chem.* **2005**, *44*, 7414–7422.
(44) Simaan, A. J.; Boillot, M. L.; Riviere, E.; Boussac, A.; Girerd, J. J. *Angew. Chem., Int. Ed.* **2000**, *39*, 196–198.

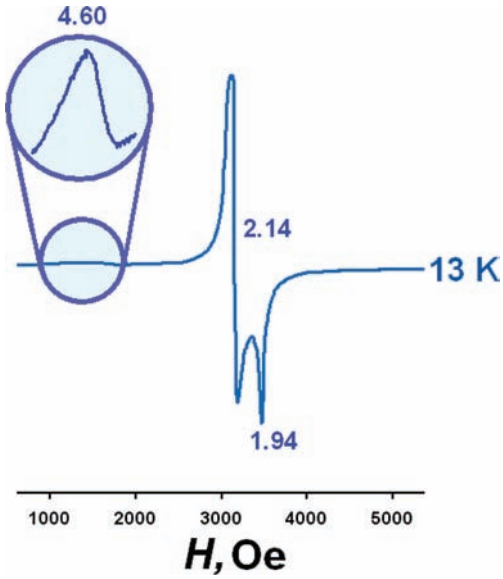

Figure 7. X-band EPR spectrum recorded at 13 K after rapid cooling of the polycrystalline sample showing the trapped HS Fe(III) species (zoomed-in portion of the spectrum).

to compound **1** in the HS state, while the minor peak (Figure 6) suggests the presence of a small amount of LS species. These EPR data are in agreement with the magnetic susceptibility results. Actually, the experimental $\chi_M T$ value at room temperature for **1** is 4.25 cm^3 mol^{-1} K which is only slightly below the theoretical value, that is, 4.377 cm^3 mol^{-1} K,[36] for HS Fe^{III} ($S = 5/2$) species.

Rapid cooling experiments have been then carried out with the aim to trap metastable HS species. Therefore, an EPR tube containing a powdered sample of **1** was quickly inserted in the EPR cavity cooled to 13 K. The spectrum recorded at this temperature (fast cooling) is depicted in Figure 7. As is evidenced in the spectrum, a weak broad signal at $g = 4.60$ is observed together with the sharp signals corresponding to the LS state ($g_\perp = 2.14$ and $g_\parallel = 1.94$), as obtained by slow cooling of the sample (see Figure 6, spectrum recorded at 70 K). The signal at $g = 4.60$ obviously corresponds to the HS state of **1** (see the room temperature spectrum in Figure 6), which has been (partially) thermally trapped. The integration of the HS and the LS signals gives rise to a HS/LS ratio of 1/14.5 (namely 6.5% of the iron(III) species are in the HS state). This value is consistent with the HS/LS percentage, that is, about 7%, found by trapping the HS state in the SQUID device (see Figure 5 and Experimental Section).

Such thermal trapping has been well investigated by Mössbauer spectroscopy[45,46] magnetic susceptibility measurements,[47−49] and X-ray diffraction.[50] However, to the best of our knowledge, this is the first example of experimental evidence of a thermal spin-state trapping proven by EPR spectroscopy.

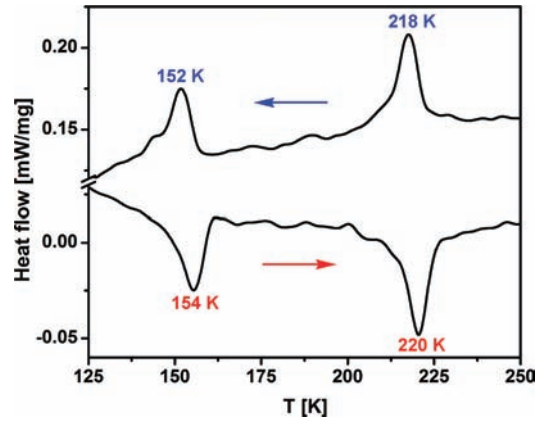

Figure 8. DSC analysis for **1**.

Table 4. ^{57}Fe Mössbauer Parameters for **1**[a]

T (K)	HS fraction (%)	δ (mm s^{-1})	Δ (mm s^{-1})	LS fraction (%)	δ (mm s^{-1})	Δ (mm s^{-1})
250	**100**	0.449(5)	0.996(9)			
220	**47.4(2)**	0.460(1)	1.031(3)	**52.6(2)**	0.135(6)	2.564(1)
190	**46.6(3)**	0.470(9)	0.980(2)	**53.4(3)**	0.151(4)	2.468(8)
110				**100**	0.166(2)	2.583(4)
80				**100**	0.172(2)	2.591(4)

[a] δ and Δ stand for the isomer shift (relative to metallic iron at room temperature) and the quadrupole splitting, respectively (error bars are given in parentheses).

Differential Scanning Calorimetry. DSC measurements for **1** were carried out in the temperature range 125−250 K at a rate of 10 K min^{-1}. The temperature dependence of the heat flow in the cooling and heating modes is shown in Figure 8. The anomalies in the heat flow for compound **1** appear in the cooling mode at $T^1_{c\downarrow} = 218$ and $T^2_{c\downarrow} = 152$ K and at $T^2_{c\downarrow} = 154$ and $T^1_{c\downarrow} = 220$ K in the warming mode. These values agree reasonably well with those observed from the $\chi_M T$ versus T plot (Figure 5). These transition temperatures determined by DSC are in reasonably good agreement with the magnetic data. The average changes in enthalpy (ΔH) values associated with these thermal anomalies are 7.0 kJ mol^{-1} (T^1_c) and 6.3 kJ mol^{-1} (T^2_c) (the values are given per metal ion involved in each step of the transition.). The corresponding entropy gains (ΔS), calculated from these thermal anomalies using the relation $\Delta H = T\Delta S$ are 31 J mol^{-1} K^{-1} (T^1_c) and 42 J mol^{-1} K^{-1} (T^2_c). These values are in the range of the expected values for spin transitions in Fe^{III} compounds.[51] It is interesting to notice that the systematic appearance of a shoulder on the low-temperature side of the main peaks (reminiscent to some extent of the shape of the magnetic curves) may be an indication of an additional structural transformation accompanying the SCO.

Mössbauer Spectroscopy. ^{57}Fe Mössbauer spectra of **1** were recorded as a function of temperature in the range 80−300 K. Spectral parameters are given in Table 4 and selected spectra are displayed in Figure 9. At 295 K, a strongly asymmetric quadrupole doublet is observed, which

(45) Garcia, Y.; Ksenofontov, V.; Mentior, S.; Dirtu, M. M.; Gieck, C.; Bhatthacharjee, A.; Gütlich, P. *Chem.—Eur. J.* **2008**, *14*, 3745–3758.
(46) Buchen, T.; Gütlich, P.; Goodwin, H. A. *Inorg. Chem.* **1994**, *33*, 4573–4576.
(47) Halcrow, M. A. *Polyhedron* **2007**, *26*, 3523–3576.
(48) Roubeau, O.; deVos, M.; Stassen, A. F.; Burriel, R.; Haasnoot, J. G.; Reedijk, J. *J. Phys. Chem. Solids* **2003**, *64*, 1003–1013.
(49) Yu, Z.; Liu, K.; Tao, J. Q.; Zhong, Z. J.; You, X. Z.; Siu, G. G. *Appl. Phys. Lett.* **1999**, *74*, 4029–4031.
(50) Marchivie, M.; Guionneau, P.; Létard, J. F.; Chasseau, D.; Howard, J. A. K. *J. Phys. Chem. Solids* **2004**, *65*, 17–23.
(51) Floquet, S.; Boillot, M. L.; Riviere, E.; Varret, F.; Boukheddaden, K.; Morineau, D.; Negrier, P. *New J. Chem.* **2003**, *27*, 341–348.

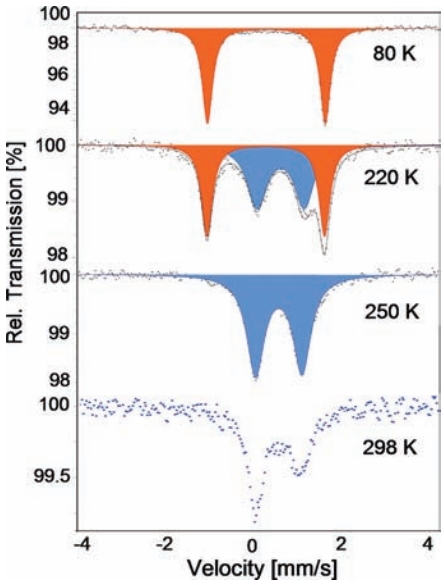

Figure 9. ^{57}Fe Mössbauer spectra of a polycrystalline sample of **1**. The HS Fe^{III} doublet is shown in blue, and the LS Fe^{III} doublet in orange.

cannot be fitted by a "static spectrum". The appearance of such relaxation spectra is a widespread phenomenon for iron(III) SCO compounds and indicates that the spin-interconversion rate of **1** is of the same magnitude than the time scale of the ^{57}Fe Mössbauer effect (ca. $10^{-6}-10^{-8}$ s).[19] At 250 K, the interconversion rate is slower, and one can observe a fairly symmetric quadrupole doublet, which can be fitted by Lorentzian lineshapes. The hyperfine parameters (isomer shift $\delta = 0.449$ mm s^{-1} and quadrupole splitting $\Delta E_Q = 0.996$ mm s^{-1}) characterize the iron(III) species in the HS state ($S = 5/2$).[52] As the temperature is decreased to 220 K, a new doublet emerges at the expense of the original HS doublet. This new signal, with $\delta = 0.135$ mm s^{-1} and $\Delta E_Q = 2.564$ mm s^{-1} is ascribed to a LS iron(III) species,[29,30] which obviously results from a HS-to-LS transition. The ratio HS/LS at this temperature is about 1:1 (Table 4) which is in agreement with the magnetic susceptibility data (Figure 5). At 190 K, δ and ΔE_Q values comparable to those found at 220 K are obtained (Table 4), thus illustrating the occurrence of a wide [HS-LS] plateau, as determined as well by SQUID measurements (see above). With further decreasing of the temperature to 110 K, the HS doublet disappears, and the remaining doublet, with $\delta = 0.166$ mm s^{-1}and $\Delta E_Q = 2.583$ mm s^{-1}, is due to LS iron(III) species ($S = 1/2$).[53]

The variation of the relative fraction of both doublets (corresponding to HS and LS species) with the temperature clearly confirms the presence of a two-step spin-transition in **1** and corroborates the results of the temperature-dependent magnetic susceptibility measurements.

Concluding Remarks

The mononuclear iron(III) compound **1** obtained from 2-methoxy-6-(pyridine-2-ylhydrazonomethyl)phenol (**Hmph**), containing both hydrogen-donor and hydrogen-acceptor groups, and iron(II) perchlorate in methanol exhibits two-step, SCO properties, as revealed by susceptibility measurements, spectroscopy, and X-ray crystallography. The abrupt character of the transitions is remarkable as it has been rarely reported in the literature for iron(III) SCO complexes. Another remarkable feature is the wide temperature range (ca. 45 K) where the [HS-LS] intermediate state is stable. The lattice hydrogen-bonding contacts induced by the well-designed ligand give rise to steep transitions (as compared with an earlier reported, structurally related system), which characterize good cooperativity between the SCO centers. This cooperativity can also explain the fact that HS species of **1** can be trapped and analyzed at low temperature by rapid cooling in an EPR cavity. Indeed, such metastable states are difficult to observe for ferric SCO systems because of the relatively fast interconversion rates when compared to ferrous complexes.

Acknowledgment. COST Action D35/0011 and coordination by the FP6 Network of Excellence "Magmanet" (contract number 515767) are kindly acknowledged. The Advanced Light Source is supported by the Director, Office of Science, Office of Basic Energy Sciences, of the U.S. Department of Energy under Contract No. DE-AC02-05CH11231. J.K. acknowledges the National Natural Science Foundation of China (Grants 20841001 and 20871113).

Supporting Information Available: Crystallographic data for **1** in CIF format. Temperature dependence of the unit cell volume *V* of **1** at different temperatures (Figure S1) and representation of the single-crystal X-ray structure of **1** with the cell axes (Figure S2). This material is available free of charge via the Internet at http://pubs.acs.org.

IC801973X

(52) Floquet, S.; Simaan, A. J.; Riviere, E.; Nierlich, M.; Thuery, P.; Ensling, J.; Gütlich, P.; Girerd, J. J.; Boillot, M. L. *Dalton Trans.* **2005**, 1734–1742.

(53) Alonso, P. J.; Martinez, J. I.; Garcia-Rubio, I. *Coord. Chem. Rev.* **2007**, *251*, 12–24.